# Dynamic Computed Tomography, an algebraic reconstruction method with deformation compensation

Sofia Ntalampeki
MSc student in Informatics,*
University Joseph Fourier, Grenoble 1
Laboratory TIMC, Equipe GMCAO
In3S, Medical Faculty
38706 La Tronche
France
email: sofia_dala@yahoo.gr

Supervisor: Laurent Desbat (Laurent.Desbat@imag.fr)

15 June 2007

*Master Franco-Hellenic in Informatics, University of Crete, Heraklion, Greece

# Acknowledgements

I am extremely grateful to my supervisor, Laurent Desbat, for giving me the opportunity to work in this interesting field of dynamic tomography, for his valuable help and support during my research work in the laboratory.

I would also like to thank very much Emmanouel Promayon, for his valuable help and advice during my research work, especially in the computer graphics part of my work.

I wish to thank Simon Rit and David Sarrut, from the team RIO (Rayonnement, Images, Oncologie) of Léon Bérard Center in Lyon, for their welcoming in an interesting meeting about dynamic tomography that took place in Lyon last February 2007.

I would also like to thank the team coordinator of GMCAO, Jocelyne Troccaz for her hospitality.

A "grand merci" to all the members of the team GMCAO, the PhD students, the Msc students for their hospitality and kindness. It was a great experience for me to work with this team.

I would also like to thank Saddek Bensalem, the coordinator of the Master Franco-Hellenique in Grenoble, and Joseph Sifakis from VERIMAG laboratory, for their support at the beginning of my studies in Grenoble.

Finally, I wish to thank the people from the department of International Relations of University Joseph Fourier and Master IVR (Imagerie, Vision, Robotique) for their hospitality during this year of my postgraduate studies in France.

## Laboratory TIMC-IMAG[1]

The laboratory Techniques de l'Ingéniere Médicale et de la Complexité (TIMC-IMAG), concentrates on the use of computer science and applied mathematics for understanding and controlling normal and pathological processes in biology and healthcare. This multi-disciplinary activity both contributes to the basic knowledge of those domains and to the development of systems for computer-assisted diagnosis and therapy.

## Team GMCAO[2]

The team Gestes Médico-Chirurgicaux Assistés par Ordinateur (Computer Assisted Medical Interventions), has a clinical objective, to assist the physician or surgeon in the successful execution of diagnostic or therapeutic gestures by minimizing invasiveness whilst improving accuracy. Some of its currect research projects are about dynamic tomography, endoscopic surgery, computer-assisted prostate biopsies, soft tissus modelisation, data and statistical models for human skull geometry.

[1] http://www-timc.imag.fr/
[2] http://www-timc.imag.fr/rubrique9.html

# Contents

# List of Figures

# 1 Introduction

## 1.1 Medical imaging

Medical imaging is an important tool for diagnostic medicine, which provides the way to visualize the inner part of the body of an organism, which is invisible. There are several imaging modalities which provide the necessary information through the medical images that they construct. According to the kind of desirable information the medical images can be distinguished in two main types:

1. Structural images: which show anatomical structures and they are obtained from:
    - Magnetic Resonance Imaging (MRI), uses the properties of the magnetic field for the diagnosis, it is considered as one of the most accurate imaging method,
    - X-rays, the radiography, which is based on the use of ionizing electromagnetic radiation,
    - Computed Tomography (CT), uses the X-rays to acquire a slice image in two dimensions (2D) or a volume in three-dimensions (3D).
2. Functional images: which analyze a specific function performed in a specific area of the human body and they are acquired from the techniques of nuclear medicine,
    - Single Photon Emission Computed Tomography (SPECT), in which the section acquisition is based on the use of $\gamma$-rays
    - Positron Emission Tomography (PET), which produces a three-dimensional image or a map of functional processes in the body.

The above categorization between imaging modalities and medical image type is not strictly defined. Nowadays, there are modalities which can provide both structural and functional information, such as functional MRI (used in neuroimaging). All imaging modalities have the same desired goals, as for example to provide medical images with high resolution and to reduce the number of artifacts.

Fig. 1: "A modern tomography scanner"

In the rest of this research work, we concentrate on Computed Tomography and more particularly in Dynamic CT, for which we consider a dynamic reconstruction taking into account the compensation (or correction) of the existed deformations.

## 1.2 Computed Tomography

The first CT scanner was invented by Hounsfield in 1972, for this invention he and Cornack were awarded in 1979 with the Nobel Prize. This invention was a great revolution in diagnostic medicine, giving the possibility to inspect human's anatomy with not an invasive way. The function of this first scanner was based to a large number of measurements, in order to reconstruct a cross-sectional slice of the patient's body. Since that time, there were invented different kinds of scanners according to the existed scanning parameters. The progress of CT was very tightly related with the development of computer power and reconstruction techniques.

The most well-known technique of CT is the 2D slice-based CT, which has been in clinical use for many years. However, the need for more accuracy and better visualization have motivate the interest of today's science to the 3D or volumetric CT and also to the development of more efficient reconstruction approaches considering the dynamic nature of human body.

## 1.3 Dynamic Computed Tomography

In dynamic tomography, we consider dynamic organs which have both time evolution and motion. The purpose of dynamic CT is to reconstruct tomographic image sequences of these dynamical organs in order to take into account the dynamic nature of a living human body. The main applications are:

- cardiac imaging, to study heart kinetic or to reconstruct coronary arteries,
- 3D CT fluoroscopy for image-guided intervention, to help the radiologist to guide a biopsy needle through soft tissues like lungs,
- radiotherapy planning to better delineate tumours and healthy tissues during motion and to determine the boundaries of the regions they are moving inside,
- in modalities of nuclear medicine such as PET or SPECT because of long measurement time.

### 1.3.1 Cardiac Imaging

Nowadays, the diagnosis and therapy of cardiac diseases are considered crucial matters, as heart disease is one of the most frequent reasons of death. There are many modalities for cardiac imaging which are categorised in two main categories,

- *Invasive*, referred to angiograms which require the insertion of a catheter into a peripheral artery and with the help of a radio contrast agent, the visualization is possible.
- *Non-invasive*, including:
  - Ultrasons, an ultra-sound based imaging technique, in order to visualize muscles and internal organs, their size, structures and possible pathologies.
  - Nuclear imaging,
  - Magnetic Resonance Imaging,
  - Computed tomography,

The respiratory and cardiac motions during CT causes artifacts, such as blur, streaks and bands which are obvious in the acquired images. These artifacts can mimic disease and lead to misdiagnosis. The existing methods in order to reduce these artifacts either modify the scanning protocols or the reconstruction algorithm. For the first case reducing the scanning time it is believed that it can reduce the artifacts but, on the other hand this can cause lower signal-to-noise ratio.
Synoptically, the magnitude of the artifacts is affected by:

- the scanning time,
- the temporal relationship between data acquisition and the respiratory cycle,
- the initial angle of the X-ray source.

There are several algorithms for respiratory motion correction that have been proposed in the literature. One of them, is the approach of Crawford et al.[1] where the respiration, in an object cross-section, is described by a time-varying magnification and displacement model (see Fig.2). Ritchie et al.[17] refined their method, assuming that the motion model is correct only in a small region around each object, and developed a pixel-specific filtered backprojection algorithm. Wang et al.[23] proposed a knowledge-based helical multi-slice/CBCT approach for dynamic volumetric imaging. Their approach uses the time varying anatomical information of the heart and is suitable for CBCT. McLeish et al.[24] derived a patient-specific model of the respiratory movement and the deformation of the heart's surface for the MRI imaging. It is based on relatively low-resolution pre-scans with breath holds in different positions of the respiratory cycle, and monitoring landmarks on the reconstructed surface of the heart. There are also other intersting research works about the estimation of the heart respiratory motion [25], gated cone-beam CT imaging of the thorax [10], patient's motion compensation [18] and dynamic echo-planar MRI of the diaphragm [12,13].

# 2 Basic tools for Computed Tomography

In tomography, we are interested in, the reconstruction of a cross-section in 2D or a volume in 3D from the acquired projections. The object function

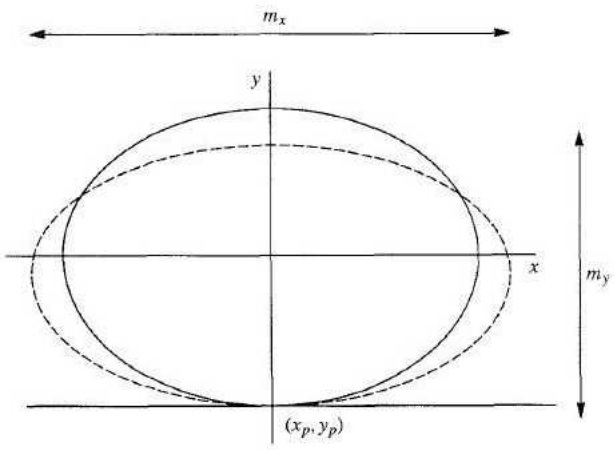


Fig. 2: "In Crawford's approach, the outline of a cross section of a patient's chest during respiration. The time-varying magnification about the $x$ and $y$ axes, denoted by $m_x$ and $m_y$ respectively, with the fulcrum of this magnification at the point $(x_p,y_p)$ which is the point where the patient's back is resting on the scan table. The solid and dashed lines represent different samples in the respiratory cycle [1]."

which is wanted to be reconstructed, is modeled as a 2D (or respectively 3D) distribution of the X-ray attenuation function and a line integral represents the total attenuation suffered by a beam of X-rays as it travels in a straight line through the object [26]. Each line is expressed by the ($\theta$,$t$) parameters, where $\theta$ is the angle and $t$ the smallest distance to the origin of the coordinate system:

$$xcos\theta + ysin\theta = t \tag{1}$$

and the relative X-ray transmission along some path is given by the line integral:

$$P_\theta(t) = \int_{(\theta,t)line} f(x,y)ds \tag{2}$$

The above result, can also be explained with the *Beer's law* which is referred to the intensities values, if $I_0$ is the intensity of the X-ray from the origine, and $I_d$ is the intensity of the rayon in the point $d$ of the detector, from the Beer's law we have:

$$I_d = I_0 \cdot e^{-\int_0^d f(x)dx} \tag{3}$$

If we take the logarithm in (3), we have the following form for the attenuation function $f(x)$, which is the same as in (2)

$$\ln\left(\frac{I_0}{I_d}\right) = \int_0^d f(x)dx \tag{4}$$

## 2.1 The Radon Transform

In 1917, J. Radon proved mathematically, that the reconstruction of 2D and 3D objects from their multiple projections was possible. Using the Dirac $\delta$-function in (2), the Radon transform is

$$P_\theta(t) = \int_{-\infty}^{\infty}\int_{-\infty}^{\infty} f(x,y)\delta(xcos\theta + ysin\theta - t)dxdy \tag{5}$$

In the context of tomography, the Radon transform data is often called a *sinogram*, because the Radon transform of a delta function is the characteristic function of a sine wave. In $n$-dimensions, the Radon transform is the integral of a function over hyperplanes. The inverse of the Radon transform is used to the reconstruction of images.

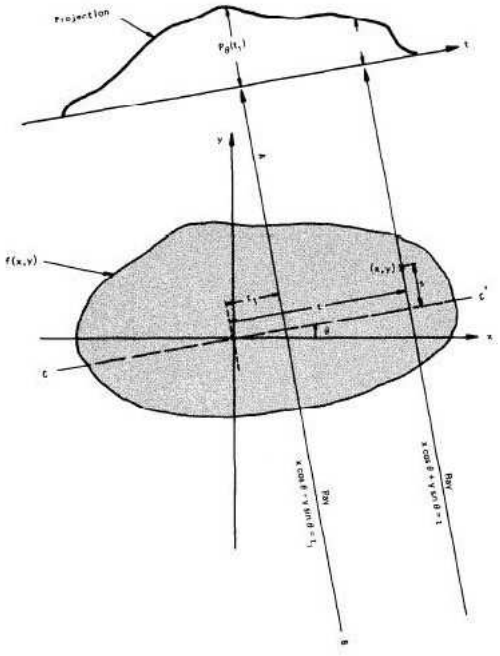


Fig. 3: "The Radon Transform"

## 2.2 The Fourier-Slice Theorem

The Fourier slice theorem is derived by taking the 1-D Fourier transform of a parallel projection and noting that is equal to a slice of the 2-D Fourier transform of the original object. The two-dimensional Fourier transform is defined by:

$$F(u,v) = \int_{-\infty}^{\infty}\int_{-\infty}^{\infty} f(x,y)e^{-j2\pi(ux+vy)}dxdy \tag{6}$$

The 1-D Fourier transform of the line integral $P_\theta(t)$

$$S_\theta(w) = \int_{-\infty}^{\infty} P_\theta(t)\ e^{-j2\pi wt}dt$$

then

$$S_\theta(w) = F(w,\theta) = F(w\cos\theta, w\sin\theta)$$

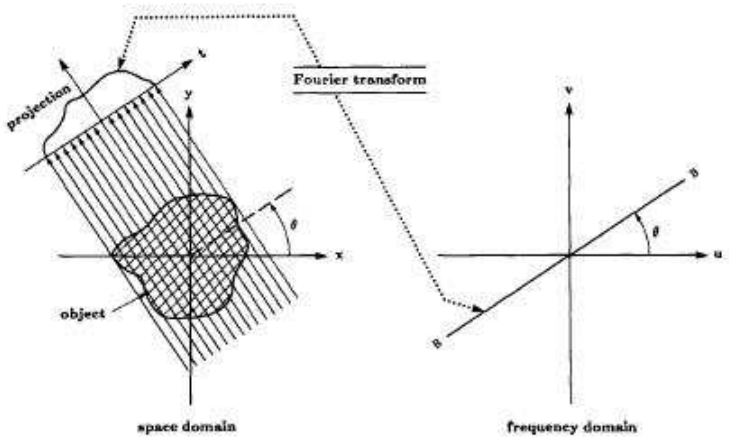


Fig. 4: "The Fourier-slice Theorem"

Given to an infinite number of projections, then $F(u, v)$ would be known at all points of the $uv$-plane, and the object function $f(x, y)$ can be recovered by using the inverse Fourier transform:

$$f(x, y) = \int_{-\infty}^{\infty} \int_{-\infty}^{\infty} F(u, v) e^{j2\pi(ux+vy)} du dv \tag{7}$$

## 2.3 Scanning Geometry

In reconstruction algorithms, the rays geometry contributes to a more efficient data acquisition. In tomography, there are three main kinds of rays beams:

- The *parallel-beam case*, which is a collection of parallel ray integrals $P_\theta(t)$ as is given in (2) for a constant angle $\theta$ . It could be measured by moving an X-ray source and detector along parallel lines on opposite sides of an object [26](see Fig.5).

- The *fan-beam case*, where a single source is placed in a fixed position relative to a line of detectors. It is called fan-beam projection because the line integrals are measured along fans (see Fig.6) [26].

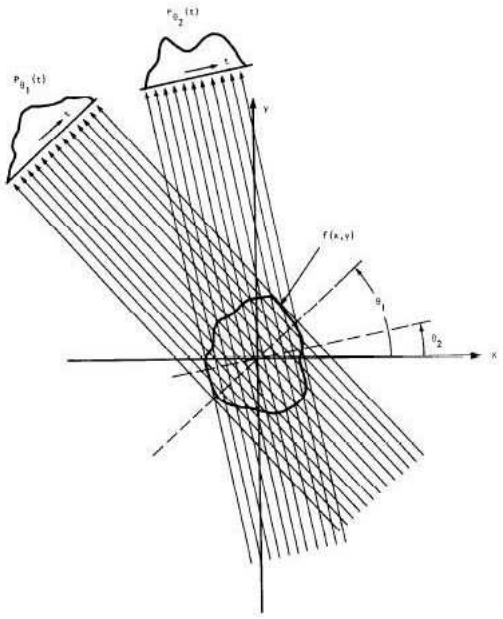

Fig. 5: "The parallel-beam geometry"

- The *cone-beam case*, where the entire object is illuminated with a point source and the X-ray flux is measured on a plane. The rays form a cone shape, as shown in Fig.8, for that reason is called cone beam reconstruction. In this case, more X-rays are able to penetrate the object, and if a 2D detector is considered, all image data in the image originate from the same time instance, that enables easy gated imaging, and then image-based methods can be used for 3D reconstruction. This is why nowadays there is a lot of interest in cone beam approaches [26].

## 2.4 Techniques of reconstruction

In computed tomography, we are interested in the reconstruction of the attenuation function from its projections. There are two types of reconstruction methods that are mainly used in CT:

1. Analytical methods, which are focused to the Fourier slice theorem,
2. Algebraic methods, which solve the reconstruction problem by solving a system of simultaneous linear equations.

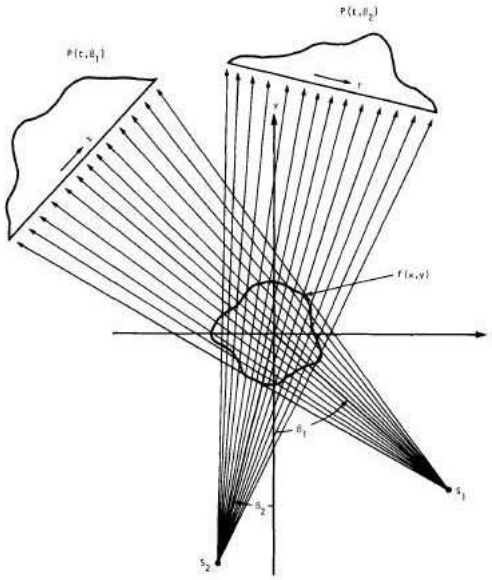

Fig. 6: "The fan-beam geometry"

### 2.4.1 Analytical Methods

In this category, we have the filtered backprojection algorithm which is nowadays the standard algorithm of tomography [4,9]. A very challenging problem in 3D tomography, is to have a reconstruction algorithm which is both efficient and theoretically exact. Katsevich [3,11] proposed a theoretically exact inversion formula for Spiral CT, which is based to the filtered backprojection algorithm. In this proposed method, firstly, there is a shift-invariant filtering of a derivative of the cone beam projections, and secondly, the result is back-projected in order to form an image. Katsevich's algorithm suffers from artifacs due to discretization and/or sampling errors, and not from the non-exacteness of the reconstruction scheme. Another commonly used algorithm in cone beam tomography is the Feldkamp algorithm [31].

In the context of dynamic CT, there are related works considering analytic compensation of deformations. The deformation compensation is incorporated within the analytical reconstruction algorithms for time dependent deformations defined as $\vec{\Gamma}_t$, in 2D parallel and fan beam tomography [2], (generalized in 3D [28]) and also in dynamic 3D Cone Beam tomography

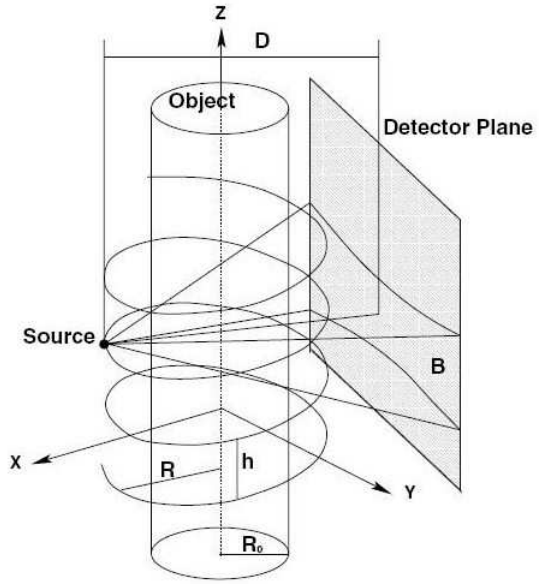


Fig. 7: "The cone-beam geometry, in helical cone-beam CT. In this scanning configuration, $D$ is the distance between the X-ray source and the detector, $R_0$ is the maximum radius of the object, the $R$ and $h$ describe the helix, in the 3D Cartesian coordinate system fixed on the object where $h$ denotes the pitch length that is the distance between consecutive turns and $R$ is the distance between the X-ray source and the rotation center [9]"

[27]. In the case where $\vec{\Gamma}_t$ is an affine transformation [2], so it preserves parallelism and intersections, it is considered that a parallel-beam projection is transformed into another parallel-beam projection and in fan-geometries, a fan-beam projection is transformed into another fan-beam projection. In [27], the $\vec{\Gamma}_t$ is considered to preserve globally the cone beam aquisition geometry, where the set of convergent lines are transformed into another set of convergent lines.

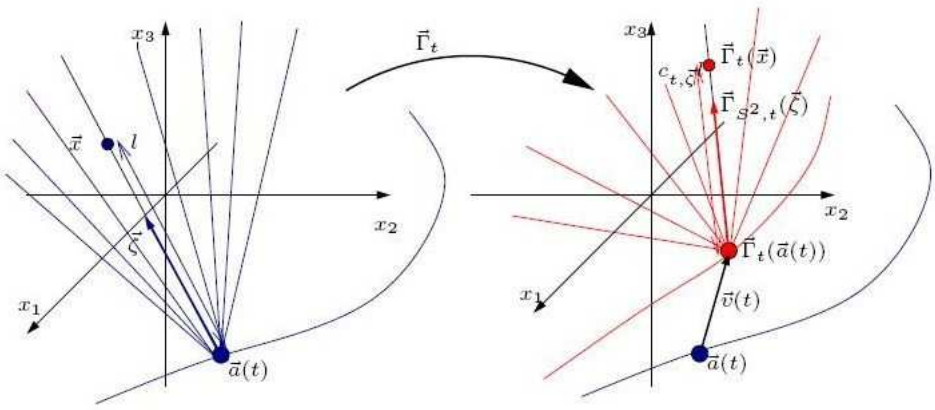


Fig. 8: "The deformation $\vec{\Gamma}_t$ in 3D Cone Beam tomography, the $\vec{\zeta} \in S^2$ is a unit vector (where $S^2$ is the unit sphere in $\mathbb{R}^3$ and a unit circle in $\mathbb{R}^2$, respectively), $\vec{a}(t) \in \mathbb{R}^3$ is the X-ray source position at time $t \in T \subset \mathbb{R}$, $t$ is then also the source trajectory parameter in $\mathbb{R}^3$, [28]"

### 2.4.2 Algebraic Methods

The Algebraic Reconstruction Technique (ART) was proposed by Gordon, Bender, and Herman as a method for the reconstruction of three-dimensional objects from electron-microscopic scans and X-ray photography. The Fourier methods that existed in that time, were rather limited in the reconstruction of objects and also had many computational requirements. However, Fourier methods matured quickly and nowadays are considered as one of the most frequent way of reconstruction.

In algebraic methods, the reconstruction is done by solving a system of linear equations. More precisely, ART can be written as a linear algebra

problem, $\mathbf{WF} = \mathbf{P}$, where $F$ is the unknown ($N \times 1$) column vector storing the values $(f_1, ..., f_N)$ of all $N = n^2$ *surface elements* or pixels in 2D or $N = n^3$ *volume elements* or voxels in 3D respectively, in the reconstruction grid. So, the image is represented as a single point in a $N$-dimensional space. $\mathbf{P}$ is the ($M \times 1$) column vector composed of the $p_i$ values that represent the ray-sum measured with the $i$th ray (see Fig.9), where $M$ is the total number of rays in all acquired projections. Finally, $\mathbf{W}$ is the ($M \times N$) weight (coefficient) matrix in which an emlement $w_{ij}$ represents the contribution of the $j$th cell to the $i$th ray integral. The factor $w_{ij}$ is equal to the fractional area of the $j$th image cell intercepted by the $i$th ray as shown for one of the cells in Fig.9 . The most of the $w_{ij}$'s are zero since only a small number of cells contribute to any given ray-sum. In 3D the $w_{ij}$ is a measure of the influence that voxel $f_j$ has on the ray $r_i$ passing through the pixel $p_i$ . The linear system can be written as follows:

$$\begin{aligned} w_{11}f_1 + w_{12}f_2 + w_{13}f_3 + ... + w_{1N}f_N &= p_1 \\ w_{21}f_1 + w_{22}f_2 + w_{23}f_3 + ... + w_{2N}f_N &= p_2 \\ & \\ w_{M1}f_1 + w_{M2}f_2 + w_{M3}f_3 + ... + w_{MN}f_N &= p_M \end{aligned} \tag{8}$$

In the above linear system, each of the above equations represents a hyperplane. When a unique solution to these equations exists, the intersection of all these hyperplanes is a single point ginving that solution. If $M$ and $N$ were small, we could use conventional matrix theory methods to invert the system of equations in the above linear system. However, in practise $N$ may be as large as 65.000 (for $256 \times 256$ images), and in most cases for images of this size, the number of rays $M$ in all the projections will have also the same size. In this case the size of the matrix $[w_{ij}]$ is large enough which precludes any possibility of direct inversion. When noise is present in the measurement data and when $M < N$, even for small $N$ it is not possible to use direct matrix inversion and some least squares methods may have to be used. Also, when $M > N$, an overdetermined system with the presence of measurement noise, in this case there is not a unique solution.

In the common case, where $M$ and $N$ have large values, there exist very attractive iterative methods to solve (8), as the direct inversion is computational impractical. These iterative methods are based on the "method of

projections" as first proposed by *Kaczmarz*, and later elucidated further by *Tanabe* [26]. Firstly, an initial guess of the solution $\vec{f}^{(0)}$ is considered in the N-dimensional space, where in most cases it is simply assigned a value of zero to all $f_i$'s. This compuatational procedure starts with the initial guess for the solution, then taking the succesive projections on the hyperplanes represented by the equations in (8), eventually yielding $\vec{f}^{(M)}$. In the next iteration, $\vec{f}^{(M)}$ is projected on the hyperplane represented by the first equation in (8) and then succesively onto the rest hyperplanes in (8) to yield $\vec{f}^{(2M)}$, and so on. The process is mathematically described by:

$$\vec{f}^{(i)} = \vec{f}^{(i-1)} - \frac{(\vec{f}^{(i-1)} \cdot \vec{w}_i - p_i)}{\vec{w}_i \cdot \vec{w}_i} \vec{w}_i \tag{9}$$

where $\vec{w}_i = (\vec{w}_{i1}, ..., \vec{w}_{iN})$, and $\vec{w}_i \cdot \vec{w}_i$ is the dot product of $\vec{w}_i$ with itself.

About the convergence of the algorithm, *Tanabe* has shown that if there exists a unique solution $\vec{f}_s$ to the system of equations in (8), then

$$\lim_{k \to \infty} \vec{f}^{(kM)} = \vec{f}_s \tag{10}$$

In algebraic methods, it is proved mathematically that we need fewer projections than for the analytical methods [29]. There are also other Algebraic Reconstruction methods,

- Simultaneous ART (SART), is considered efficient in implementation and the most accurate between algebraic methods [26].
- Simultaneous Iterative Reconstruction Technique (SIRT) [26].

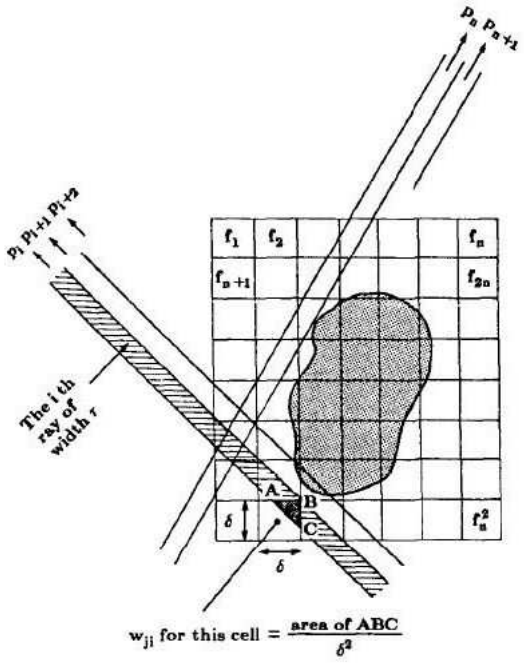


Fig. 9: "Algebraic methods, where a square grid is superimposed over the unknown image. Image values are assumed to be constant within each cell of the square grid.[26]

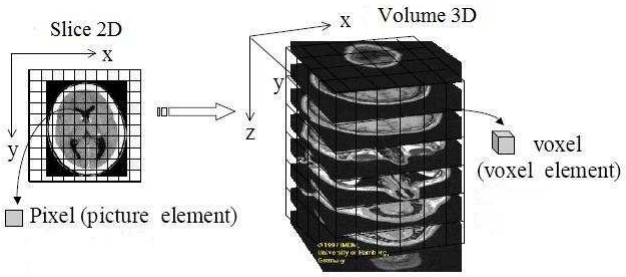


Fig. 10: "In 2D the cross-section is referred to pixels and in 3D we consider voxels, which are pixels in three-dimensions. In 3D CT the 3D object is represented as a stack of seperately reconstructed 2D slices."

# 3 The proposed dynamic algebraic reconstruction method

In this research work, we concentrate on the 3D cone beam tomography problem. The object function $f : \mathbb{R}^3 \to \mathbb{R}$ is the 3D attenuation distribution to be reconstructed from the projections which are acquired from the imaging modalities such as Computed Tomography, SPECT or PET. We consider the 3D cone beam transform:

$$g_D(t, \vec{\zeta}) \stackrel{def}{=} Df(t, \vec{\zeta}) \stackrel{def}{=} D_t f(\vec{\zeta}) \stackrel{def}{=} \int_0^{+\infty} f\left(\vec{a}\,(t) + \lambda\vec{\zeta}\right) d\lambda \qquad (11)$$

where $\vec{\zeta} \in S^2$ is a unit vector in $\mathbb{R}^3$ ($S^2$ is the unit sphere in $\mathbb{R}^3$), $\vec{a}(t) \in \mathbb{R}^3$ is the X-ray source position at time $t \in T \subset \mathbb{R}$, $t$ is then also the source trajectory parameter in $\mathbb{R}^3$ . $D_t f(\vec{\zeta})$, at fixed $t$, is supposed to be acquired in a negligible time, $\forall \vec{\zeta} \in S^2$. The function $f$ is supposed to have a compact support and $\vec{a}(t)$ has a strictly positive distance to the support of $f$. Then, $\vec{\zeta}$ is the direction joining the source $\vec{a}(t)$ to a pixel on the X-ray detector producing the scalar measurement $D_t f(\vec{\zeta})$.

This transform appears in 3D X-ray Computed Tomography (reconstruction from 2D X-ray projections or multiline CT) with application in cardiac imaging or radiotherapy. In this 3D cone beam tomography problem the desired result is the reconstruction of the attenuation distribution $f$ from the cone beam projections $g_D$.

## 3.1 The proposed deformation model

One of the problems presented in Computed Tomography as already mentioned in section 1.3, is the presence of artifacts due to movement or deformations that occur. In dynamic tomography, the attenuation function $f$ to be reconstructed is also a function of the time $t$. In this approach, we consider a time dependent deformation of the space as in [1], [5]. For this time dependent deformation model $\vec{\Gamma}_t$ it is assumed that, for $t \in T$, $\vec{\Gamma}_t$ are known bijective appropriately smooth functions on $\mathbb{R}^3$ whose inverse are smooth too, $\vec{\Gamma}_t$ is a diffeomorphism.

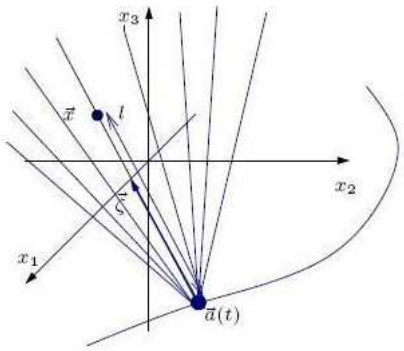


Fig. 11: "The Cone-Beam parameters"

We assume that the attenuation function $f$ at point $\vec{x} \in \mathbb{R}^3$ at time $t$ can be written in the form $f_{\vec{\Gamma}_t}(\vec{x}) = f\left(\vec{\Gamma}_t(\vec{x})\right)$, where $f$ is the attenuation reference point (for example, at reference time $t = 0$). Thus, $\vec{\Gamma}_t$ simply transforms the position $\vec{x}$ at time $t$ to its position $\vec{\Gamma}_t(\vec{x})$ at the reference time ($t = 0$).

The problem to consider is the reconstruction of $f$, or equivalently of $f_{\vec{\Gamma}_t}$ from cone beam measurements, $Df_{\vec{\Gamma}_t}$, for a known deformation function $\vec{\Gamma}_t$. Our objective is to apply efficient accurate deformation corrections in the reconstruction algorithms.

In 2D case the deformation function $\vec{\Gamma}_t$ is written:

$$\begin{aligned} \vec{\Gamma} &: \mathbb{R}^2 \to \mathbb{R}^2 \\ &\vec{x} \to \vec{\Gamma}(\vec{x}) \end{aligned}$$

$$\begin{aligned} \Gamma_1 &: \mathbb{R}^2 \to \mathbb{R} \\ &\vec{x} \to \Gamma_1(\vec{x}) = y_1 \\ \Gamma_2 &: \mathbb{R}^2 \to \mathbb{R} \\ &\vec{x} \to \Gamma_2(\vec{x}) = y_2 \end{aligned} \tag{12}$$

Where $\vec{x} = (x_1, x_2) \in \mathbb{R}^2$, $\vec{y} = (y_1, y_2) \in \mathbb{R}^2$. $\vec{y}$ gives the position of $\vec{x}$ in the reference time $t$.

A more general definition in $n$ dimensions for the deformation $\vec{\Gamma}_t$ is:

$$\begin{aligned} \vec{\Gamma} \ &: \mathbb{R}^n \to \mathbb{R}^n \\ &\vec{x} \to \vec{\Gamma}(\vec{x}) \end{aligned}$$

$$\begin{aligned} \Gamma_i \ &: \mathbb{R}^n \to \mathbb{R} \\ &\vec{x} \to \Gamma_i(\vec{x}) \ = \ y_i \end{aligned} \tag{13}$$

where $i \in [1, ..., n]$ and $\vec{x} = (x_1, ..., x_n) \in \mathbb{R}^n$, $\vec{y} = (y_1, ..., y_n) \in \mathbb{R}^n$

## 3.2 The algebraic approach

In this approach [30], we suppose that the unknown function $f$ can be decomposed into a finite linear combination of given independent functions, such as voxel indicator (or pixel indicator) functions in $\mathbb{R}^3$ or in $\mathbb{R}^2$ respectively. Let $(e_j)_{j \in J}$ be a set of basis functions $e_j : \mathbb{R}^3 \to \mathbb{R}$, $J$ being a finite set of index such as $J = \{1, ..., n_J\}, n_j \in \mathbb{N}$ denoting the number of elements $\#(J)$ of the set $J$ (multi index sets are also very often used in multi dimensional space). For example, $e_j$ can be the indicator function of the voxel number $j$ in the reconstruction region. We assume that a good approximation of the continuous function $f(\vec{x})$, is obtained by using the basis functions $e_j$, as follows:

$$f(\vec{x}) = \sum_{j \in J} f_j e_j(\vec{x}), \text{ where } f_j \in \mathbb{R}, \ j \in J \tag{14}$$

We also suppose now that the acquisition can be modelled by

$$d_i = \int_\Omega h_i(\vec{x}) f(\vec{x}) d\vec{x}, \ i \in I \tag{15}$$

In 2D tomography, $h_i(\vec{x})$ could be the Dirac $\delta$-function on a line $\delta(\vec{x} \cdot \theta_i - s_i)$ where $\theta$ is the direction of the projection and $s \in \mathbb{R}$ is the signed distance of the line to the center. In 3D $h_i(\vec{x})$ could be the Dirac $\delta$-function on the X-ray line but it could also be the indicator of the conical region joining a point source $\vec{a_i}$ and a detector or some smooth version obtained by calibration of the X-ray, PET or SPECT system. In nuclear imaging, $h_i$ can also model more physics such as attenuation, etc. The number of data $n_I$ is finite.

In static tomography, the algebraic approach yields to solve a linear system

$$\begin{aligned} d_i &= \int_\Omega h_i(\vec{x}) f(\vec{x}) d\vec{x} \\ &= \int_\Omega (h_i(\vec{x}) \sum_{j \in J} f_j e_j(\vec{x}) d\vec{x}) \\ &= \sum_{j \in J} \left( \int_\Omega h_i(\vec{x}) e_j(\vec{x}) d\vec{x} \right) f_j \\ &= \sum_{j \in J} A_{ij} f_j \end{aligned} \tag{16}$$

We have to solve the linear system $\mathbf{d} = \mathbf{Af}$ where $\mathbf{d} = (d_i)_{i=1,\ldots,n_I}$ is the known vector of data, $\mathbf{f} = (f_j)_{j=1,\ldots,n_J}$ is the unknown vector of coefficients of $f$ to be identified and the matrix entry $A_{i,j}$ is $A_{i,j} = \int_\Omega h_i(\vec{x}) e_j(\vec{x}) d\vec{x}$ which represents the line integral of the basis function $e_j(\vec{x})$ along the $i$th ray. The matrix is generally sparse because both $h_i$ and $e_j$ functions have a limited support in the domain $\Omega \subset \mathbb{R}^3$. For the solution of the linear system in (16), we can use iterative methods.

In the section 2.4.2, the linear system (8) is the same as in (16). The form of (16) reduces to (8) if for $e_j$'s we use the following pixel basis (or voxel basis in $3D$ respectively), which is obtained by dividing the image frame into $N$ identical subsquares (or subcubes in 3D, respectively), these are referred to as pixels (or voxels in 3D) and identified by the index $j$ for $1 \leq j \leq N$:

In 2D, where $\vec{x} \in \mathbb{R}^2$, the pixel basis is

$$e_j(\vec{x}) = \begin{cases} 1, & \text{when } \vec{x} \text{ is inside the jth pixel} \\ 0, & \text{everywhere else.} \end{cases} \tag{17}$$

In 3D, where $\vec{x} \in \mathbb{R}^3$, the voxel basis is

$$e_j(\vec{x}) = \begin{cases} 1, & \text{when } \vec{x} \text{ is inside the jth voxel} \\ 0, & \text{everywhere else.} \end{cases} \tag{18}$$

In (14) the $f_j$'s with these basis functions $e_j(\vec{x})$ represent the average of $f(\vec{x})$ over the $j$'th pixel and $A_{i,j}$ represents the length of intersection of the $i$th ray with the $j$th pixel when we assume that rays have zero width. Otherwise if we associate a finite width with each ray, the elements of the projection matrix will represent the areas of intersection of these ray strips with the pixels (or voxels in 3D).

In dynamic tomography, the acquisition is modeled as

$$\begin{aligned} d_{t,i} &= \int_\Omega h_i(\vec{x}) f(\vec{\Gamma}_t(\vec{x})) d\vec{x} \\ &= \sum_{j\in J} \left( \int_\Omega h_i(\vec{x}) e_j\left(\vec{\Gamma}_t(\vec{x})\right)\right) f_j \end{aligned} \tag{19}$$

Like before, we have for the basis function:

$$e_j(\vec{\Gamma}_t(\vec{x})) = \begin{cases} 1, & \text{when } \vec{\Gamma}_t(\vec{x}) \text{ is inside the jth pixel} \\ 0, & \text{everywhere else.} \end{cases} \tag{20}$$

Respectively for 3D,

$$e_j(\vec{\Gamma}_t(\vec{x})) = \begin{cases} 1, & \text{when } \vec{\Gamma}_t(\vec{x}) \text{ is inside the jth voxel} \\ 0, & \text{everywhere else.} \end{cases} \tag{21}$$

Now we suppose that the functions $e_j\left(\vec{\Gamma}_t(\vec{x})\right)$ can be decomposed (or approximated) into a finite linear combination of given independent functions $(b_k)_{k\in K}$, $K$ being a finite index (or multi-index) set, more precisely

$$e_j(\vec{\Gamma}_t(\vec{x})) = \sum_{k\in K} \Gamma_{t_{k,j}} b_k(\vec{x}) \tag{22}$$

then (22) introduced in (19) yields to

$$\begin{aligned} d_{t,i} &= \sum_{j\in J} \left( \int_\Omega h_i(\vec{x}) \sum_{k\in K} \vec{\Gamma}_{t_{k,j}}(\vec{x}) b_k(\vec{x}) d\vec{x} f_j \right) \\ &= \sum_{j\in J} \left( \sum_{k\in K} \left( \int_\Omega h_i(\vec{x}) b_k(\vec{x}) dx \right) \vec{\Gamma}_{t_{k,j}}(\vec{x}) \right) f_j \end{aligned}$$

$$= \sum_{j\in J}\left(\sum_{k\in K} B_{i,k}\Gamma_{t_{k,j}}\right) f_j \tag{23}$$

where $\mathbf{B}$ is the algebraic matrix for the basis functions $(b_k)_{k\in K}$

$$B_{i,k} = \int_\Omega h_i(\vec{x}) b_k(\vec{x}) dx \tag{24}$$

In 3D CB tomography, $i$ is usually a multi-index, at least one index, say $i_1$, is related to the source position on its trajectory, and an other index (or multi-index) $i_2$ is related to the detector pixel position in space at the source position $i_1$ or equivalently the direction of the ray from the source position at $t(i_1)$ (usually, in 3D CB, $i_2$ is a multi-index of two values because the direction space $S^2$ is a two-dimensional set). Thus $t$ is a function of $i_1$ (the time at the source position), and $d_{t,i}$ is $d_{t(i_1),i_2}$, where $i = (i_1, i_2), i_1 \in I_1, i_2 \in I_2$, $I = I_1 \times I_2$ and

$$\begin{aligned} d_{t(i_1),i_2} &= Df_{\vec{\Gamma}_{t(i_1)}}\left(t(i_1), \vec{\zeta}(i_2)\right) \\ &= \sum_{j\in J}\left(\sum_{k\in K} B_{(i_1,i_2),k}\Gamma_{t(i_1)_{k,j}}\right) f_j \end{aligned} \tag{25}$$

Thus,

$$\mathbf{d_{i_1}} = \mathbf{B_{i_1}}\mathbf{\Gamma_{t(i_1)}}\mathbf{f},\ i_1 = 1, ..., n_{I_1} \tag{26}$$

where the $n_{I_1}$ matrices $\mathbf{B_{i_1}}$ are $n_{I_2} \times n_K$ ($n_{I_1}$ sets of $n_{I_2}$ lines of a classical ART matrix corresponding to each $i_1$ source position, $i_1 = 1, ..., n_{I_1}$) and the matrices $\mathbf{\Gamma_{t(i_1)}}$ are $n_K \times n_J$ matrices coding the deformations by $\vec{\mathbf{\Gamma}}_{\mathbf{t(i_1)}}$ of the basis functions $e_j$ into the basis functions $b_k$, for each considered time $t(i_1)$, $i_1 = 1, ..., n_{I_1}$. With this formulation, an algebraic matrix for dynamic tomography differs from the classical algebraic method only by the introduction of the matrices $\mathbf{\Gamma_{t(i_1)}}$. Just as for classical tomography, iteratives methods are used for solving the linear system (23) and the matrices $\mathbf{B}$ and $\mathbf{\Gamma_{t(i_1)}}$, $i_1 = 1, ..., n_{I_1}$ are generally not stored but computed during the iterations.

## 3.3 Deformation compensation

The desired result, of this research work is to identify the matrices $\mathbf{\Gamma_{t(i_1)}}$, $i_1 = 1, ..., n_{I_1}$ that code the deformations in the dynamic algebraic reconstruction

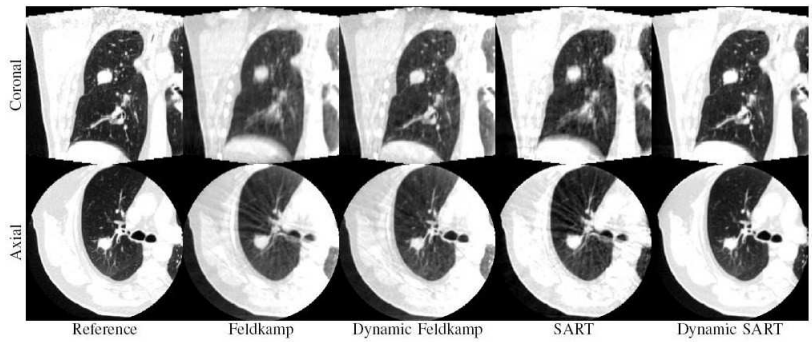


Fig. 12: "Coronal and axial slices of the reconstruction results on the realistic digital phantom of the thorax. Feldkamp and SART methods do not take into account the motion. Dynamic Feldkamp uses a heuristic compensation of the motion during the backprojection step of Feldkamp algorithm. Dynamic SART is identical to the SART method taking into account the motion"

method.

### 3.3.1 Deformations in medical images

In medical imaging, as in image processing, for image registration we compute the transformation that is related to the points, in one image to their corresponding points in the other. This type of transformation can be:

- global or local,
- rigid or deformable.

Rigid-body transformations, have limited application because many organs deform substantially. Thus, this type of transformation is considered in the cranium and brain imaging, but is not valid within the abdomen, pelvis, thorax or extremities. Internal structures, such as the heart, do enlarge and contract due to normal physiological functions, so the region of interest does not necessarily maintain a fixed relationship to bony structures. For most organs in the body, many more degrees of freedom are needed to describe the different deformations with adequate accuracy.

In the case of *elastic registration* [15], the techniques can be categorized as point-based and voxel-based methods. Point-based techniques minimize the distance between features such as points, curves or surfaces of corresponding anatomical structures. They require the identification and matching of these features on both reference and test images. This process usually needs certain amount of human interactions. After point-matching, the remaining procedure of registration is only interpolation or approximation. Voxel-based methods use similarity measures such as the sum of squared distance, cross-correlation or mutual information between images. They have the advantage that they do not require any feature extraction process.

A synoptical categorization of the main deformations kinds, according to the kind of geometry that they present given in [22]:

1. Euclidean geometry, (rigid deformations)
2. Similarity geometry,
3. Affine geometry, (affine transformation)
4. Projective geometry,
5. Inversive geometry,
6. Differential geometry (diffeomorphism),
7. Topological geometry.

### 3.3.2 The proposed deformation compensation

In this dynamic algebraic reconstruction method, we consider a general type of deformation, as already mentioned in section 3.3.1 which belongs to the non-trivial case of non-linear deformations. Deformations which are linear, such as rigid and affine deformations, can be easily implemented in the reconstruction process due to the linearity properties that they have. For example, in the case of rigid deformations, it is possible to use virtual source and detector positions and apply the reconstruction algorithm as in the static case or to deform the data before reconstruction.

In our general case, we want to identify the deformations matrices $\mathbf{\Gamma_{t(i_1)}},\ i_1 = 1, ..., n_{I_1}$ , which describe the deformations by $\vec{\mathbf{\Gamma}}_{\mathbf{t(i_1)}}$ of the basis functions $e_j$ into the basis functions $b_k$ for each considered time $t(i_1)$ $i_1 = 1, ..., n_{I_1}$. In the reconstruction process, the intersection of the straight acquisition line with $f_{\vec{\Gamma}_t}(\vec{x})$ should take into account the translation and the deformation of the basis functions.

We suppose that $f(\vec{x}, t) = f_{\vec{\Gamma}_t}(\vec{x}) = f(\vec{\Gamma}_t(\vec{x}))$, which means that the attenuation function at time $t$ is the same with the attenuation function at the reference time in $\vec{\Gamma}_t(\vec{x})$ (the attenuation function is not changed by $\vec{\Gamma}_t$).

In 2D we have the basis functions (as already defined in section 3.3.2),

$$\begin{aligned} e_j : \mathbb{R}^2 &\rightarrow \mathbb{R} \\ \vec{x} &\rightarrow e_j(\vec{x}) \end{aligned}$$

$$\begin{aligned} b_k : \mathbb{R}^2 &\rightarrow \mathbb{R} \\ \vec{x} &\rightarrow b_k(\vec{x}) \end{aligned} \tag{27}$$

The $b_k(\vec{x})$ are considered as pixel indicators, like $e_j(\vec{x})$. We have assumed that $e_j(\vec{\Gamma}_t(\vec{x}))$ are approximated, by the linear combination of $b_k$'s,

$$e_j(\vec{\Gamma}_t(\vec{x})) = \sum_{k \in K} \Gamma_{t_{k,j}} b_k(\vec{x}) \tag{28}$$

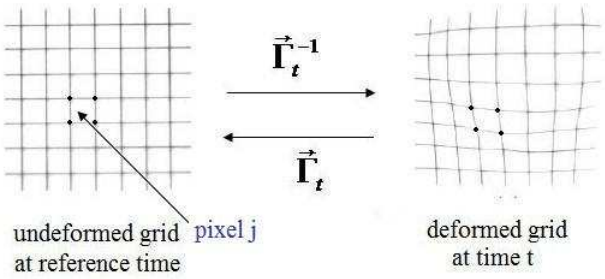


Fig. 13: "Grid deformation"

$\vec{\Gamma}_t$ transforms the point $\vec{x}$ to $\vec{\Gamma}_t(\vec{x})$ at the reference time ($t = 0$). In the definition of the deformation model, we have assumed that the $\vec{\Gamma}_t$ is a diffeomorphism, so it is bi-regular and bijective, and its inverse $\vec{\Gamma}_t^{-1}$ can be defined. $\vec{\Gamma}_t^{-1}$ is referred to the deformation from the position $\vec{\Gamma}_t$ at reference time to the position $\vec{x}$ at time $t$ (see Fig.13), and is supposed to be known. We have also assumed that,

$$e_j(\vec{\Gamma}_t(\vec{x})) = \begin{cases} 1, & \text{when } \vec{\Gamma}_t(\vec{x}) \text{ is inside the jth pixel} \\ 0, & \text{everywhere else.} \end{cases} \tag{29}$$

Thus, from (29), we have that, $e_j(\vec{\Gamma}_t(\vec{x})) = 1$ *iff* $\vec{x} \in \vec{\Gamma}_t^{-1}(pixelj)$

Indeed, in dynamic tomography, the movements (deformations) that occur during the projections acquisition do not preserve the geometry of the acquisition lines. We make the assumption that the boundary of the reconstruction grid is invariant.

We consider two grids, the regular (*undeformed grid*) at the reference time, and a irregular (*deformed grid*) at time $t$, see Fig.13. The $e_j(\vec{\Gamma}_t(\vec{x}))$ can be calculated, by deforming the pixel $j$ of the regular grid with the $\vec{\Gamma}_t^{-1}$ and taking the indicator of that pixel in the deformed grid.

For the identification of the deformations, a regular grid described with the $b_k$ functions is superimposed over the deformed grid. We could approximate the deformations of this pixel $j$ by finding for which $k$ the $\Gamma_{kj}$ is zero (there is no deformation) and where is non-zero (there is deformation).

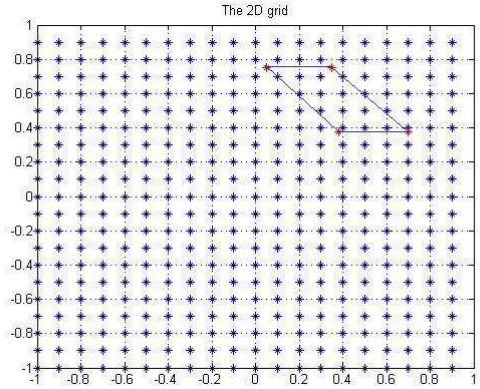


Fig. 14: "A 2D grid, with $20 \times 20$ grid points, where the red coloured points (not necessary grid points) describe the position of a deformed pixel calculated by $\vec{\Gamma}_t^{-1}$"

In Fig.14, a simple example using Matlab, we have the grid which is described with $b_k$'s and the pixel $j$ which has been deformed by the $\vec{\Gamma}_t^{-1}$. In order to approximate the deformation, we look for the intersections of the pixel $j$ with $b_k$'s. The surface which represents these intesections (polygons in 2D) is the approximated deformation.

In 3D the problem is more complex because the intersections between the deformed voxels and the voxels of the regular grid, represent more complex shapes such as polyhedrons. In that case the deformations could be approximated with the volume that describes this intersection.

# 4 Conclusions - Further work

Dynamic tomography is a very active and well-promising domain of research in diagnostic medicine. The desired result of a dynamic 3D cone beam reconstruction algorithm, which is an image with a quality comparable to CT images of static objects, can provide many benefits to the clinical diagnosis and research.

In this research work, a theoretical base for a 3D cone beam dynamic algebraic reconstruction algorithm has been presented. The proposed deformation compensation, could give the desired results to the deformation compensation problem.

# References


[1] "Respiratory compensation in projection imaging using a magnification and displacement model", Carl R.Crawford, Kevin F.King, Cameron J.Ritchie and J.David Godwin, *IEEE Trans. Med. Imaging, 15, no.3, June 1996.*

[2] "Compensation of some time dependent deformations in tomography", Laurent Desbat, Sébastien Roux and Pierre Grangeat.

[3] "Theoretically exact FBP-type inversion algorithm for spiral CT", Alexander Katsevich.

[4] "Image reconstruction from fan-beam projections on less than a short scan", Frédéric Noo, Michel Defrise, Rolf Clackdoyle and Hiroyuki Kudo, *Phys.Med.Biol.47 (2002) 2525-2546.*

[5] "Exact reconstruction in 2D dynamic CT: compensation of time-dependent affine defomormations", Sébastien Roux, Laurent Desbat, Anne Koening and Pierre Grangeat, *Phys.Med.Biol.49 (2004) 2169-2189.*

[6] "Computable elastic distances between shapes", Laurent Younes.

[7] "Optimal matching between shapes via elastic deformations", Laurent Younes.

[8] "Invariance, deformations et reconnaissance de formes", Mathematiques et Applications. Springer-Verlag L.Younes.

[9] "Reconstruction from minimum data in helical cone-beam CT", Yu Zou and Xiaochuan Pan.

[10] "Gated cone-beam CT imaging of the thorax: a reconstruction study", Simon Rit, David Sarrut and Serge Miguet.

[11] "A general scheme for constructing inversion algorithms for cone beam CT", Alexander Katsevich.

[12] "Functionnal model of the diaphragm for computer assisted medical interventions", E.Promayon, L.Gaillard and S.Craighero.

[13] "Dynamic echo-planar MR imaging of the diaphragm for a 3D dynamic analysis", S.Craighero, E.Promayon, P.Baconnier, J.F.Lebas and M.Coulomb.

[14] "Elastic registration of medical MR images", Lars Kristian Nielsen, *University of Bergen.*

[15] "Fast free-form deformable registration via calculus of variations", Weiguo Lu, Ming-Li Chen, Gustavo Olivera, Kenneth J.Ruchala and Thomas R.Mackie, *Phys.Med.Biol.49 (2004) 3067-3087.*

[16] "Image deformation using Moving Least Squares", Scott Schaefer, Travis McPhail and Joe Warren.

[17] "Correction of computed tomography motion artifacts using pixel-specific back-projection", Cameron J.Ritchie, Carl R.Crawford, J.David Godwin, Kevin F.King and Yongmin Kim, *IEEE Trans. Med.Imaging, 15, no.3, June 1996.*

[18] "Theoretical framework for a dynamic cone-beam reconstruction algorithm based on a dynamic particle model", Pierre Grangeat, Anne Koenig, Thomas Rodet and Stéfane Bonnet, *Phys.Med.Biol.47 (2002) 2611-2625.*

[19] "Elastic registration of medical MR images", Lars Kristian Nielsen, *Thesis in Computer Science, University of Bergen, January 2003.*

[20] "3D Simultaneous Algebraic Reconstruction Technique for Cone Beam projections", Wojciech Chlewicki, *Master of Science Thesis, University of Patras, 2001.*

[21] "Cone Beam reconstruction using Filtered Backprojection", Henrik Turbell, *Thesis in Computer Science, Sweden, 2001.*

[22] "The Mathematical Description of Shape and Form", E.A.Lord and C.B. Wilson.

[23] "A knowledge-based conebeam x-ray CT algorithm for dynamic volumetric cardiac imaging", Wang Ge, Zhao Shiying, Heuscher Dominic, *Med.Phys.2002;29;1807-22.*

[24] "A study of the motion and deformation of the heart due to respiration", McLeish Kate, Hill Derek L.G., Atkinson David, Blackall Jane M., Razavi Reza, *IEEE Trans. Med.Imaging 2002;21:1142-50.*

[25] "Estimation of the heart respiratory motion with applications for Cone Beam Computed Tomography imaging; a simulation study", Ivan G.Buliev, Cristian T.Badea, Zoi Kolitsi and Nicolas Pallikarakis, *IEEE Trans.Information Technology in Biomedicine, December 2003.*

[26] "Principles of Computerized Tomographic Imaging", Avinash C.Kak, Malcom Slaney, *IEEE Press.*

[27] "Compensation de déformations en tomogrpahie dynamique 3D conique", Laurent Desbat, Sébastien Roux, Pierre Grangeat, *Octobre 2006.*

[28] "Modèles dynamiques en tomographie, application à l'imagerie cardiaque", Sébastien Roux, *PhD Thesis, Université Joseph Fourier, Grenoble I, France, 2004.*

[29] "Fast and accurate three-dimensional reconstruction from cone-beam projection data using algebraic methods", K.Mueller, *PhD Thesis, The Ohio State University, 1998.*

[30] "Algebraic and analytic reconstruction methods for dynamic tomography", L.Desbat, S.Rit, R.Clackdoyle, C.Mennessier, E.Promayon, S.Ntalampeki, *IEEE Engineering in Medicine and Biology Conference, Lyon, France, 2007 (to appear).*

[31] "Practical cone-beam algorithm", L.Feldkamp, L.Davis, and J.Kress, *Journal of Optical Society of America A, vol. 1, no. 6, pp. 612-619, 1984.*